Soft Matter

Drainage via stratification and nanoscopic thickness transitions of aqueous sodium naphthenate foam films

Journal:	*Soft Matter*
Manuscript ID	SM-ART-08-2021-001169.R1
Article Type:	Paper
Date Submitted by the Author:	02-Sep-2021
Complete List of Authors:	Ochoa, Chrystian; University of Illinois at Chicago, Chemical Engineering Xu, Chenxian; University of Illinois at Chicago, Chemical Engineering Martínez Narváez, Carina; University of Illinois at Chicago, Chemical Engineering Yang, William; University of Illinois at Chicago, Chemical Engineering Zhang, Yiran; University of Illinois at Chicago, Chemical Engineering Sharma, Vivek; University of Illinois at Chicago, Chemical Engineering

Drainage via stratification and nanoscopic thickness transitions of aqueous sodium naphthenate foam films

Chrystian Ochoa, Chenxian Xu, Carina D. V. Martínez Narváez, William Yang, Yiran Zhang, and Vivek Sharma*

Department of Chemical Engineering, University of Illinois at Chicago, Chicago, IL.

*Correspondence to: Vivek Sharma (E-mail: viveks@uic.edu)

Submitted on August 11, 2021; Revised on September 2, 2021.

ABSTRACT

Sodium Naphthenates (NaNs), found in crude oils and oil sands process-affected water (OSPW), can act as surfactants and stabilize undesirable foams and emulsions. Despite the critical impact of soap-like NaNs on the formation, properties, and stability of petroleum and OSPW foams, there is a significant lack of studies that characterize foam film drainage, motivating this study. Here, we contrast the drainage of aqueous foam films formulated with NaN with foams containing sodium dodecyl sulfate (SDS), a well-studied surfactant system, in the relatively low concentration regime (c/CMC < 12.5). The foam films exhibit drainage via stratification, displaying step-wise thinning and coexisting thick-thin regions manifested as distinct shades of gray in reflected light microscopy due to thickness-dependent interference intensity. Using IDIOM (interferometry digital imaging optical microscopy) protocols that we developed, we analyze pixel-wise intensity to obtain thickness maps with high spatiotemporal resolution (thickness < 1 nm, lateral ~ 500 nm, time ~ 10 ms). The analysis of interference intensity variations over time reveals that the aqueous foam films of both SDS and NaN possess an evolving, dynamic, and rich nanoscopic topography. The nanoscopic thickness transitions for stratifying SDS foam films are attributed to the role played by damped supramolecular oscillatory structural disjoining pressure contributed by the confinement-induced layering of spherical micelles. In comparison with SDS, we find smaller concentration-dependent step size and terminal film thickness values for NaN, implying weaker intermicellar interactions and oscillatory structural disjoining pressure with shorter decay length and periodicity.

INTRODUCTION

Surface-active molecules like sodium naphthenate (NaN) and sodium dodecyl sulfate (SDS) spontaneously adsorb to liquid-air (and oil-water) interfaces and reduce interfacial tension, thus lowering the energy required for forming foams (and emulsions) and decreasing the driving force for drainage.[1-4] An increasing demand for oil derivatives and progressive depletion of conventional oil fields has necessitated the production and refining of unconventional crude oils (heavy and extra-heavy), including the acidic or sour crudes that contain impurities like hydrogen sulfide, naphthenic acids (NAs), and high levels of carbon dioxide.[5-8] Naphthenic acids (NAs), the mixtures of several cyclopentyls and carboxylic acids with 4 - 20 carbon backbone, are present as 0.1 - 0.3 wt.%, and 2.0 wt.% of the American and Athabasca crudes, respectively.[7-9] Athabasca oil sands deposit,[6, 9] Angola and Congo in West Africa, the North Sea, and Venezuela have high NA containing deposits.[10] Steam decompression during the refining process leads to an increase in pH, triggering the degassing of carbon dioxide and reactions between naphthenic acid and metal salts to form sodium naphthenates (NaN) or calcium naphthenates (CaN).[5] Petroleum industry loses millions of dollars annually due to the naphthenic acid-related issues, including equipment fouling, crude oil foams, crude-oil-in-water emulsions, wettability alternation by NAs, and naphthenate deposition leading to unwanted process shutdowns that interfere with flow assurance.[5, 7-13] Additional challenges and costs arise from the need for the treatment of downstream oil sands process-affected water (OSPW), [5, 14] and the role played by NaNs in stabilizing aqueous foams.[15, 16] Despite the critical impact of NaNs on the formation, drainage, and stability of foams (and emulsions), we found relatively few studies that measure their surface tension, phase behavior, and foam film drainage,[12, 17-19] motivating this study.

The few measurements show that NaN reduces the surface tension value by more than half,[12, 17-19] and displays a critical micelle concentration (CMC) in the range from c_{NaN} = 0.1-1 wt.%.[17] Surface tension assumes a constant value, and self-assembled structures called micelles spontaneously appear in bulk solutions above CMC. Taylor and coworkers[15, 16] focused on foam film drainage of a limited range of concentrations, all above CMC (5, 10, 20, 30, 40, and 50 wt.%), and found that the NaN foam films exhibit drainage by stratification. Drainage via stratification in ultrathin micellar foam films creates coexisting flat regions with distinct grayscale intensity,[20-22] and manifests as step-wise thinning in the plots of average thickness against time.[20-48] Thin film interference produces vivid, iridescent colors in soap bubbles and single foam or soap films with thickness, h > 100 nm.[1-3, 49, 50] Even though the interference intensity is still correlated with film thickness for ultrathin films with h < 100 nm, only shades of grey manifest in reflected light microscopy that gets progressively darker as the film gets thinner. [20-22, 27-51] Most stratification studies on surfactant systems, including SDS, have focused on the concentration range of $1 \leq c/\text{CMC} \leq 12.5$, which is the regime where micelles are typically spherical, and the relationship between step size and concentration can be fit by $\Delta h \sim c^{-1/3}$ or an inverse cubic root scaling.[21, 22, 27-30] In a recent contribution,[20] we extended the stratification studies for SDS to c/CMC = 30 (up to c_{SDS} = 250 mM), but we found only three other studies for c_{SDS} > 100 mM (or c/CMC > 12.5).[52-54] In contrast, Taylor et al. [7, 15, 16] focused on relatively high concentrations and described stratification for 50 wt.% NaN to be caused by the formation of a liquid crystalline phase. Therefore, the motivations for this study are three-fold: to investigate if NaN foam films with $c/\text{CMC} \leq 12.5$ (presumably $c_{NaN} \leq 12.5$ wt.%, using their CMC of c_{NaN} = 1 wt.%) stratify, to characterize concentration-dependent variation in step size and compare with scaling known for

spherical micelle formers, ($\Delta h \sim c^{-1/3}$) and lastly, to characterize the features of nanoscopic topography and underlying surface forces, as summarized next.

The drainage, stability, and lifetime of liquid foams depend on the interplay of hydrodynamic and thermodynamic forces and fluxes that drive restructuring and drainage within the intricate three-dimensional architecture of foams.[1, 2, 55-59] Thus, it is desirable to understand and control the mass flux of gases between bubbles, of liquid within thin liquid films or foam films that enclose gas pockets, and from films into Plateau borders (PBs), the thicker channels formed by intersecting films.[1-3, 57-59] The curvature gradient between liquid foam film and the PB causes a capillary / Laplace pressure gradient to contribute the impelling force for individual film drainage, whereas bulk viscous stresses primarily determine the impairing forces, though sometimes, interfacial and bulk viscoelasticity of the foaming liquid also play a role.[1-4, 33, 57-68] However, in thin films with thickness, h < 100 nm, the Laplace pressure, P_c can be counterbalanced by the thickness-dependent disjoining pressure, $\Pi(h)$ contributed by intermolecular and surface forces.[1-4, 27-30, 33, 35, 69] Therefore, the investigation of thickness transitions in a foam film undergoing drainage presents a model system to investigate the strength and range of surface forces and colloidal interactions, in addition to providing insights into foam properties and stability. For example, the combination of attractive van der Waals and repulsive electrostatic double-layer forces creates the DLVO (Derjaguin-Landau-Verwey-Overbeek) contribution to disjoining pressure, $\Pi_{\mathrm{DLVO}}(h)$ analogous to the DLVO interactions that contribute to the stability of colloidal dispersions.[1, 2, 33, 51, 69-72] The combination of steric-hydration and the DLVO forces for anionic surfactants with c < CMC leads to the formation of either ~20 nm thick common black (CB) film, or <10 nm Newton black (NB) film.[1, 2, 33, 69] However, for c > CMC, micelles present within the film undergo confinement-induced structuring that creates non-DLVO, damped, supramolecular oscillatory

structural contribution to disjoining pressure, $\Pi_{OS}(h)$ that can counterbalance P_c at multiple thicknesses, leading to stratification.[33, 35, 73, 74]

Stratification proceeds by the nucleation and growth of thinner, darker flat domains that grow at the expense of the surrounding flat film that is thicker by a quantized step-size correlated with the periodicity of $\Pi_{OS}(h)$ and the step-size observed in thickness evolution plots.[20-22, 27, 28, 33-35, 43] Even though the characterization of the nanoscopic thickness transitions and variations of stratifying freestanding films was a long-standing challenge, we developed IDIOM (interferometry digital imaging optical microscopy) protocols to facilitate thickness mapping with exquisite spatiotemporal resolution (thickness < 1 nm, lateral ~ 500 nm, time ~ 10 ms).[20-22, 27-30, 48] We used IDIOM protocols to visualize and analyze the topographical features including the growth of non-flat nanoridges and mesas that arise at the front around expanding thinner domains,[22, 27, 28] and demonstrated that the experimentally observed shape evolution of nanoridges can be modeled using thin film equation amended with $\Pi_{OS}(h)$.[22, 27, 28, 30] These studies on stratification in micellar SDS foam films establish that step size and the nanoscopic topography characterize the strength and range of intermicellar interactions and disjoining pressure, that remain unexplored for surfactants like NaN.

The manuscript is organized as follows. The measurement of surface tension is described first for NaN and SDS, primarily to determine the CMC in aqueous NaN solutions. Next, we use the IDIOM set-up and protocols to probe drainage of NaN solutions for c_{NaN} / CMC ≤ 12.5 and establish that the NaN foam films exhibit the three characteristic features of stratification we have identified for micellar SDS foam films: step-wise thinning, coexistence of thick-thin flat regions, as well as the appearance of nanoridges and mesas. We discuss the concentration-dependent variation of step-size, Δh and terminal layer thickness h_0 for NaN films, and contrast with the

corresponding values with SDS, an anionic surfactant found in many washing and cleaning products, whose properties like micelle size and shape, aggregation number, intermicellar distance, and step-size have been studied extensively by many researchers, including the authors.[20-22, 27-30, 40, 41, 71, 75-77] We outline how the quantitative analysis of thickness variations and transitions, (h_0 , Δh, $h(x,y,t)$) suggests that in comparison with SDS, NaN exhibits smaller step size, weaker intermicellar interactions, and lower magnitude and shorter decay length for the supramolecular oscillatory structural forces that drive stratification.

MATERIALS AND METHODS

Materials. Aqueous solutions of sodium naphthenate (NaN) (Tokyo Chemical Industry Co., Ltd., 6-15-9, Toshima, Kita-ku, Tokyo, Japan, N0397, Lot DLODE-HF, CAS 61790-13-4) and sodium dodecyl sulfate (SDS) (Sigma-Aldrich Co., St. Louis, MO, L6026, >99.0%), respectively were prepared by using deionized water of resistivity 18.2 $\mathrm{M\Omega \cdot cm}$. We used the surfactants as received without further purification. Typically, naphthenates produced in-situ during oil recovery from the alkali-induced saponification of acidic crudes[5, 7, 8, 11, 15, 16, 78] refer to a class of compounds. However, according to the supplier, the sodium naphthenate (NaN) used in this study has a molecular weight of 192.234 g/mol (implying c_{NaN} of 1 wt.% equals 52 mM). In contrast, SDS has a molecular weight of 288.372 g/mol and a calculated maximum hydrocarbon chain length of 1.672 nm.

Surface tension measurement: We used maximum bubble pressure tensiometry (MBPT) to characterize the dynamic surface tension for NaN and SDS solutions for the apparent surface age, t_a in the range 10 ms-10 s.[79] The apparent surface age depends on the bubbling rate. Dynamic surface tension as a function of surface age is computed from the maximum pressure measured in

each cycle of bubble formation, growth, and release.[79, 80] Quasi-equilibrium values of surface tension were obtained by extrapolating MBPT datasets to prolonged surface age. The measured concentration-dependent variation in surface tension (from MBPT data) and the inferred values of the critical micelle concentration (CMC) match well with the values measured within the group using pendant drop tensiometry using axisymmetric drop shape analysis.[79]

IDIOM (interferometry digital imaging optical microscopy) protocols and set-up. The set-up includes a Schedluko-like cell[51], a glass or plastic tube of diameter 1.6 mm that contains a nearly plane-parallel film and its surrounding thicker meniscus emulating a foam film and a Plateau border. The cell is placed in a sealed container, with an aqueous bath added to create a saturated atmosphere and thus minimize the influence of evaporation and air currents on stratification dynamics.[3, 30] A biconcave drop is initially formed within the cell, and slow liquid withdrawal from a side-arm connected to a syringe pump allows the creation of a plane-parallel film with the desired size and initial thickness (<100 nm). The constant cell diameter, d_c, and plane-parallel film diameter, d_f determine the Laplace pressure $P_c \approx 4\gamma d_c \Big/ \left(d_c^2 - d_f^2\right)$, where γ refers to the surface tension value.[51] As the surface tension becomes nearly concentration-independent above CMC, all stratification experiments carried out for a chosen surfactant are conducted for matched capillary pressure, film size, and the cell-size, to allow for a meaningful comparison.[21, 22, 27-30, 51]

We use white light from a Fiilex P360EX portable LED light source to illuminate the film, and the intensity variations accompanying drainage in a single foam film are captured using a FASTCAM Mini UX100 high-speed camera attached to a magnification system (Navitar Zoom 6000 with an added microscope objective). Every pixel in a color image obtained by the digital camera is a composite of three intensities of red (wavelength λ = 650nm), green (λ = 546nm), and blue (λ = 470nm) light, and each color channel has intensity values in the range of 0-4095 (for a

RAW image with 12-bit depth). Using IDIOM protocols that rely on white light illumination and digital filtering to obtain simultaneous intensity maps for three wavelengths,[21, 22] we obtain pixelwise thickness measurements by using the standard interferometry equation:

$$h = \left(\frac{\lambda}{2n\pi}\right)\arcsin\left(\sqrt{\frac{\Delta}{1+4R(1-\Delta)/(1-R)^2}}\right) \quad (1)$$

Here the intensity ratio, $\Delta = (I - I_{\min})/(I_{\max} - I_{\min})$ is computed using the intensity value measured at each pixel, I, and the maximum and minimum intensity values, $I_{\max}$ and $I_{\min}$, respectively. The Fresnel coefficient, $R = (n-1)^2/(n+1)^2$ is typically computed by assuming that the refractive index, n is homogeneous and equal to the value of the bulk solutions or just water (n = 1.33) and hence, is referred to as an "effective thickness" measurement[21, 34, 35, 81, 82]. We used refractive index of water (n = 1.33) for SDS and used the measured values of refractive index n = 1.3415, 1.3509, 1.3676, 1.3859, 1.4144, and 1.4200 for 5, 10, 20, 30, 40, and 50 wt.% NaN solutions, respectively (measured by Taylor *et al.*[15, 16]), to estimate n values at relevant concentrations. However, several studies find[21, 22, 34, 35, 51, 83, 84] that negilible change in measured values (<1 nm) if calculations account for the concentration-dependent variation in refractive index or the multilayered structure of the foam film. We checked that comparable values are obtained for NaN solutions by assuming n = 1.33. The image analysis is carried out in MATLAB R2020a with our specially developed codes (available on request). Experiments are carried out at room temperature. The IDIOM protocols we introduced for mapping pixel-wise intensity into thickness was adopted by Frostad et al.[85] as dynamic film interferometry for thicker films (with interference colors), later by Beltramo and Vermant[45] for analysis of lipid films with even finer nanoscopic thickness resolution by using a 16-bit camera (we use 12-bit RAW images), and into a hyperspectral imaging method by Suja et al.[86]

RESULTS AND DISCUSSION

The surface tension of NaN and SDS solutions. Concentration-dependent variations in surface tension are shown in Figures 1a and 1b for aqueous NaN and SDS solutions, respectively. Even 0.1 wt. % of NaN in water leads to a substantial drop in surface tension (to 45 mN/m), as shown in Figure 1a. The surface tension decreases with concentration up to c = 1 wt. % and then attains a concentration-independent value of 31 mM/m, implying that the critical micelle concentration (CMC) occurs at 1 wt.%. Surface tension values were measured for the aqueous sodium naphthenate solutions, and the CMC value of c_{NaN} = 1 wt. % is comparable to three distinct measurements reported in literature[12, 17, 18], including values measured using a maximum bubble pressure tensiometer.[17]

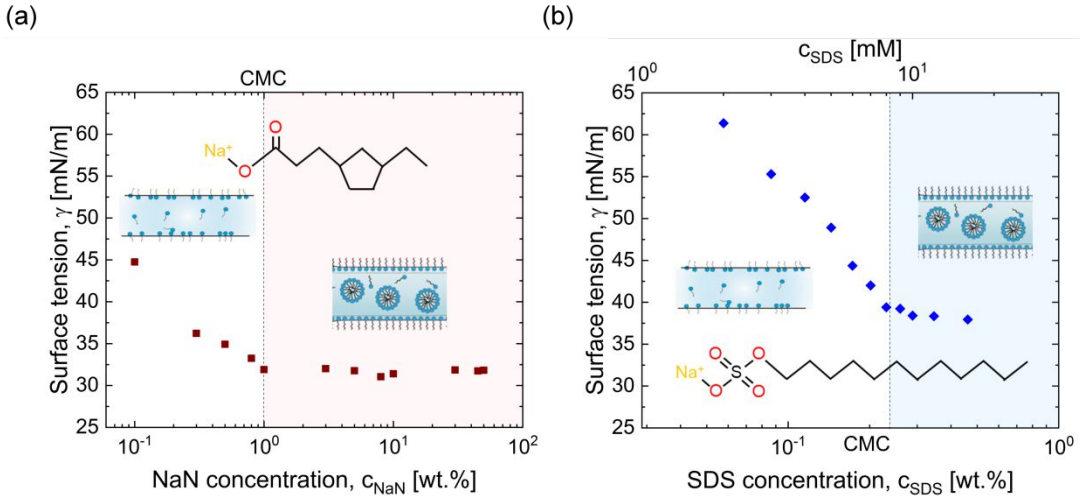

Figure 1. Concentration-dependent variation in surface tension of aqueous NaN and SDS solutions. (a) The surface tension of NaN solutions decreases with concentration before attaining a nearly constant value above c_{NaN} = 1 wt. % identified as the critical micelle concentration (CMC). For structure shown as inset, the CMC can be expressed as c_{NaN} = 52 mM. (b) Surface tension of SDS solutions exhibit a CMC of c_{SDS} = 8.2 mM (c_{SDS} = 0.24 wt.%) but the measured values of surface tension are higher than measured for NaN solutions.

A much lower value of CMC as c_{NaN} = 0.1 wt.% is attributed to Mingqing's dissertation[19] by Moran et al..[17] However, as the extraction methods and the availability of different naphthenate families can cause variations in CMC and overall surface tension values, the agreement with

published studies[12, 17, 18] appears rather striking. The surface tension measurements for aqueous SDS solutions shown in Figure 1b attain a nearly constant value of around 39 mM/m, above a CMC = 8.2 mM. More extensive literature is available for the surface tension measurements of aqueous SDS solutions,[80] and the absence of a dip near the CMC value attests to the high purity of the as-received surfactant.[87]

Step-wise thinning of foam films made with aqueous NaN and SDS solutions. Stratification in a single foam film formed in a Scheludko-like cell was visualized and analyzed using IDIOM (Interferometry, Digital Imaging, and Optical Microscopy) protocols and set-up shown schematically in Figure 2a.[21, 22, 27-30] Thickness evolution plots, shown in Figure 2 were obtained from the average intensity of a 10.4 micron-a-side square region of the foam film using the thin film interferometry equation (i.e. the equation (1)). Foam films formed with surfactant concentrations below CMC undergo drainage with a monotonic decrease in thickness. For example, in Figure 2b, the thickness evolution profile obtained for c_{NaN} = 0.1 wt.% (c_{NaN}/CMC = 0.1) exhibits a smooth decrease over time, whereas the micellar foam film with c_{NaN} = 2.5 wt.% (c_{NaN}/CMC = 2.5) displays a step-wise decrease. As Laplace pressure is kept constant and the viscosity of both solutions is quite comparable, the thickness evolution plots show that drainage via stratification delays film drainage and rupture, thus increasing the overall stability and lifetime of foams. An apparent thickness spike in the plots arises if thicker regions cross the pixels utilized for measuring the average intensity and computing the average thickness using equation 1. The thickness maps, detailed later, provide insights into the spontaneous appearance of locally thicker regions in a foam film that is undergoing stratification.

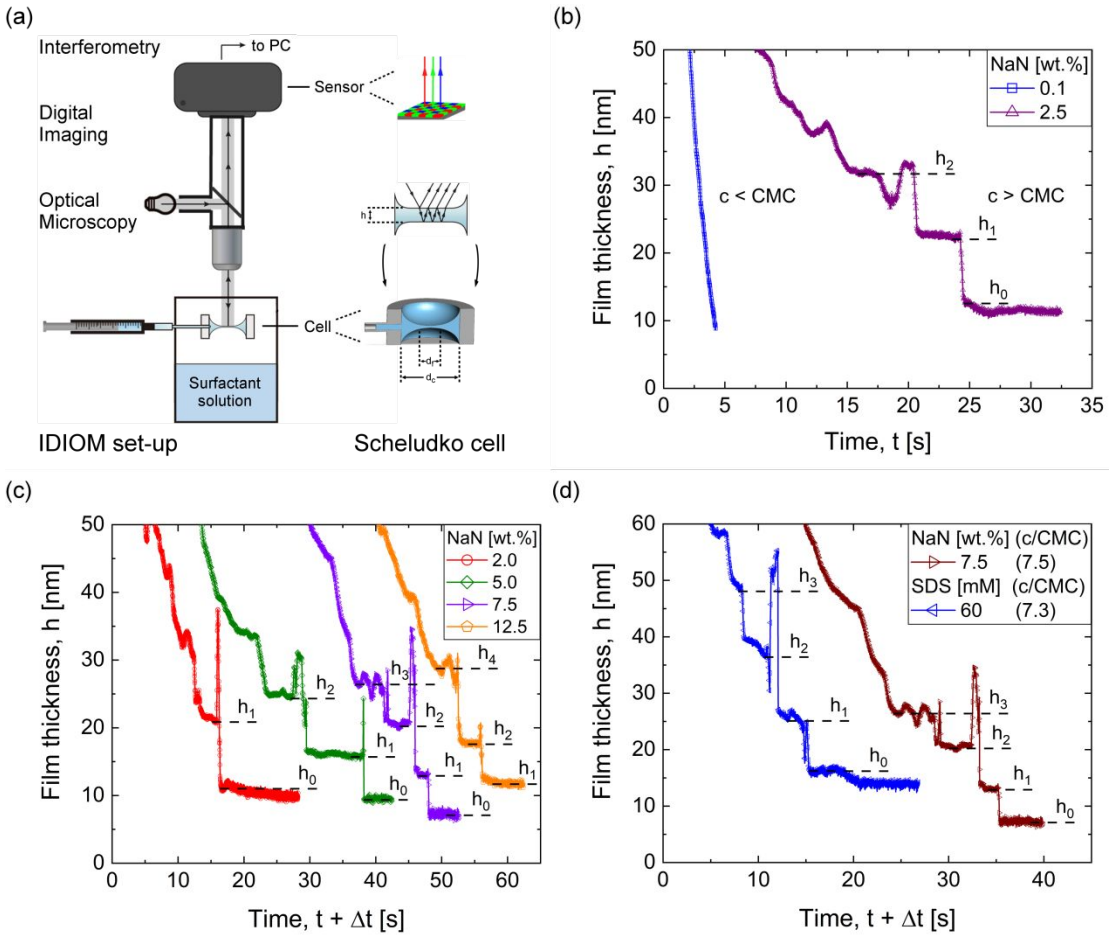

Figure 2. Step-wise thinning of NaN and SDS solutions probed using IDIOM (Interferometry, Digital Imaging, and Optical Microscopy) set-up and protocols. (a) Schematic showing IDIOM set-up. The Scheludko-like cell, placed in a closed container, contains a horizontal plane-parallel film surrounded by a thicker Plateau border. Stratification of the film is visualized using reflected light microscopy. The film's thickness variations and transitions are computed using pixel-wise measurements (2.4 pixels/micron on film surface) of spatio-temporal variation of the interference intensity $I(x, y, \lambda, t)$. **(b)** Local foam thickness obtained from the average intensity of a 10.4 micron-a-side square region is plotted as a function of time. Thickness evolution is continuous decay for c_{NaN} = 0.1 wt.% (c_{NaN}/CMC < 1), whereas for c_{NaN} = 2.5 wt.% (c_{NaN}/CMC > 1) a step-wise thinning is observed, leading to appearance of several steps or layers, labeled as h_i. **(c)** Thickness evolution plots for micellar NaN foam films with c_{NaN} = 2, 5, 7.5, and 12.5 wt.% (c_{NaN}/CMC = 2, 5, 7.5, and 12.5) exhibit step-wise thinning. Plots are shifted along the time axis for clarity. **(d)** Comparison of the thickness evolution plots for c_{NaN} = 7.5 wt.% (c_{NaN}/CMC = 7.5) and for c_{SDS} = 60 mM (c_{SDS}/CMC ≈ 7.3), shows large difference in step size and terminal film thickness. The spikes and dips in these plots of thickness over time appear due to the passage of thicker mesas or thinner domains through the selected region analyzed for computing thickness from average interference intensity.

In Figure 2c, the micellar NaN films show a concentration-dependent increase in the number of step-wise thickness transitions, *N,* and of coexisting thick-thin flat regions. Furthermore, an increase in NaN concentration leads to a decrease in the ith layer thickness, h_i, including the terminal thickness, h_0. For instance, increasing c_{NaN} = 2.5 wt.% (Figure 2b) to c_{NaN} = 7.5 wt.% (c_{NaN}/CMC = 2.5 to 7.5) in Figure 2c is accompanied by an increase in *N* from 3 to 4, and a decrease in the first layer thickness h_1 from 22 to 13 nm. For a fixed concentration, the NaN thickness evolution plots reveal a single step-size, $\Delta h = h_{i+1} - h_i$ and the step size is computed by here discounting the last step, $h_1 - h_0$. Step size progressively decreases with an increase in NaN concentration. For example, the step size decreases from 7.8 nm to 6.8 nm for an increase from c_{NaN} = 2.5 wt.% to c_{NaN} = 7.5 wt.%. Figure 2d contrasts the thickness evolution plots for micellar foam films formulated with NaN and SDS at nearly matched scaled concentration, c/CMC ≈ 7.5. Four step-wise transitions arise for both surfactants, but the stratifying SDS films display much larger thickness of the ith layer, h_i and exhibit larger step-size and terminal thickness, h_0. Here, for c_{SDS} = 60 mM (c_{SDS}/CMC ≈ 7.3), the layer h_2 thickness and step-size are 36 nm and 12.5 nm, respectively, whereas for c_{NaN} = 7.5 wt.% (c_{NaN} /CMC = 7.5), the layer h_2 thickness and step-size are 20 nm and 6.8 nm, respectively.

Next, we contrast the thickness variations accompanying drainage via stratification in foam films. Figure 3 shows image sequences that contrast the stratification process observed for foam films formulated with c_{NaN} = 2.5 wt.% and 5.0 wt.% (c_{NaN}/CMC = 2.5 and 5.0, respectively) and the corresponding thickness maps that were generated by using the IDIOM protocols. Since we have presented such topographical maps for SDS and bile salt foam films before,[20, 22, 27-30, 48] Figure 3 makes NaN the third system where such nanoscopic thickness mapping is illustrated. In reflected light microscopy, the stratifying thin films made of micellar aqueous NaN solutions exhibit distinct

shades of gray representing coexisting thick-thin regions. The lower concentration films with c_{NaN} = 2.5 wt.% exhibits three distinct shades, whereas films with c_{NaN} = 5.0 wt.% exhibits four shades.

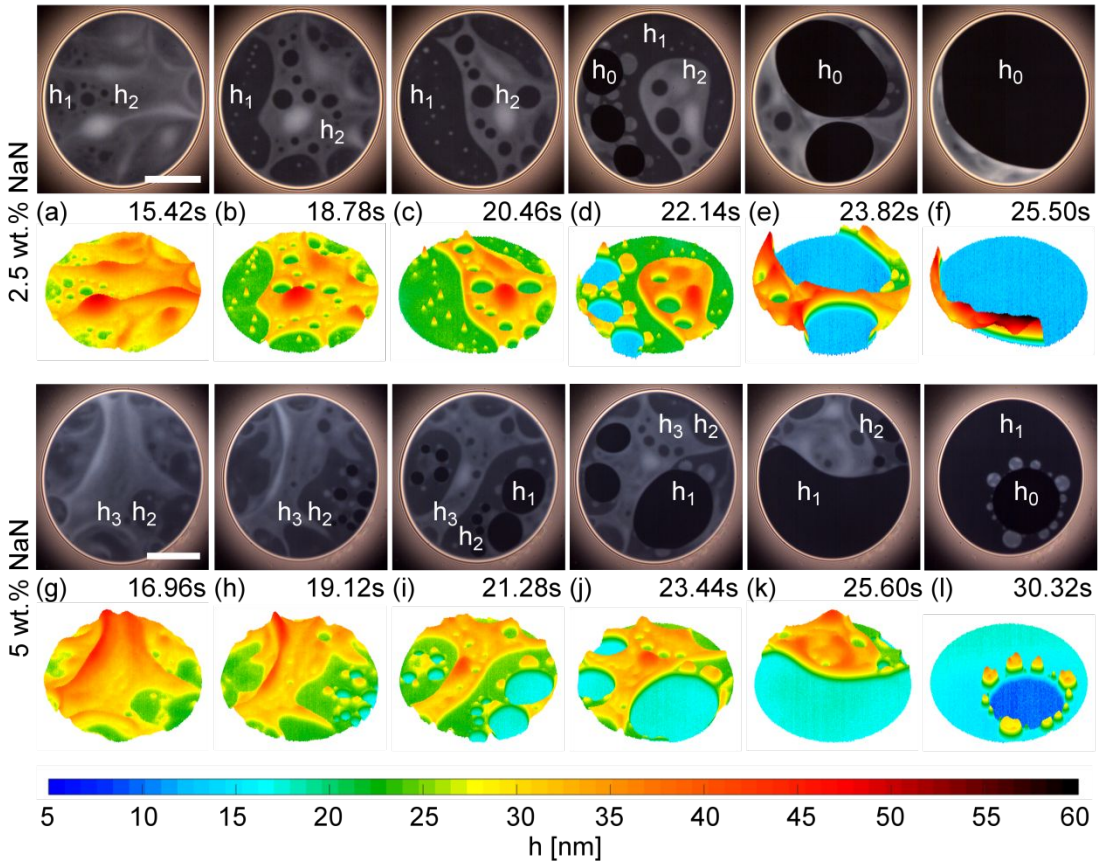

Figure 3. Coexisting shades of grays and nanoscopic topography on stratifying NaN micellar films. Image sequences show progression of stratification in micellar NaN foam films with c_{NaN} = 2.5 wt.% and 5.0 wt.% (c_{NaN}/CMC = 2.5 and 5.0 respectively). The corresponding thickness maps are obtained by using pixelwise mapping of interference intensity on to thickness using IDIOM protocols. The white scale bar, corresponding to the in-plane dimensions, is 100 μm, whereas the colormap that displays pixelwise thickness ranges from 5-60 nm. Thus, the nanoscopic topography is relatively flat. The brightness and contrast are enhanced using ImageJ for grayscale images. However, the unprocessed image in RAW format is used for analysis. The stratifying NaN foam film with c_{NaN} = 2.5 wt.% and c_{NaN} = 5.0 wt.% exhibits three and four distinct shades of gray, respectively. Isolated mesas can be observed in (b)-(d), whereas frontal mesas are present in (d), (h)-(l).

Stratification proceeds by nucleation and growth of thinner, darker domains as can be observed in the grayscale images included in Figure 3. Faint halos that form around the expanding darker domains are visualized as nanoridges in the corresponding thickness maps. Subsequently,

the nanoridges undergo a topographical instability leading to the formation of thicker, brighter white spots that are visualized as mesas around the expanding thinner domains. In these thickness maps, the in-plane length scale is in micrometers while the thickness length scale is in nanometers so that the nanoridges and mesas are relatively flat. Zhang *et al.*[27, 28] observed and characterized the topographical features that arise in stratifying SDS micellar thin films and showed that the shape evolution of nanoridges and nanoridge-mesa transition could be captured by the thin film equation amended with $\Pi_{OS}(h)$. We posit that the formation and growth of nanoridges and mesas during drainage *via* stratification of micellar NaN foam films are governed by similar mechanisms.

A spontaneous emergence of "isolated" mesas is observed in Figure 3b-3d, as contrasted with the "frontal" mesas that typically form around the expanding thinner, darker domains. Similar isolated mesas in stratifying foam films were observed by Yilixiati *et al.*[29] for salt-added SDS micellar films and more recently, by Kemal et al.[48] in micellar foam films formed with aqueous solutions of bile salts. Furthermore, Yilixiati *et al.*[29] showed that the nanoscopic topographical maps reveal the strength, range, and periodicity of $\Pi_{OS}(h)$, and described a phenomenological expression that incorporates the influence of change in Debye length, micelle number density, electrolyte concentration, and intermicellar distance (assumed equal to step-size). Yilixiati et al.[29] attributed smaller step size, formation of isolated mesas, and fewer thickness transitions to the influence of added salts, correlated with change in size, shape, and number of micelles, and a decrease in the strength of intermicellar interactions. The additional role could be played by polydispersity in micellar size, especially for stratifying foam films of bile salts, NaN, and SDS in the presence of added salt. It is well-known that bile salts self-assemble without showing a preferred micelle size or CMC due to their peculiar steroid structure, and the addition of salt increases polydispersity in size and shape for SDS micelles. However, the quantitative analysis of

micelle size, shape, and polydispersity using scattering methods and other techniques is still lacking in the literature.

In addition to micellar foam films, stratification also arises in freestanding films containing supramolecular structures like lipid layers,[44, 45] polyelectrolyte-surfactant complexes,[46, 47] nanoparticles,[40, 88] and liquid crystalline assemblies.[89] Taylor et al.[16] attributed stratification for c_{NaN} = 50 wt.%. to liquid crystallinity, as Horvarth-Szabo et al.[7] concluded that isotropic phases exist for c_{NaN} < 41.8%. Taylor et al.[15] reported that transient, localized "step-wise thickening" occurs in c_{NaN} = 45 wt.% manifested in the appearance of brighter spots, but the thickness and growth of such spots were not characterized, and the possibility of observing such localized thickening was not explored using isotropic NaN solutions. However, the formation and growth of isolated mesas shown in Figure 3 provide evidence for localized thickening in foam films made with isotropic solutions, and similar mesa formation was observed for salt-added SDS and bile salts.[29, 48] As c_{NaN} = 45 wt.% NaN solutions are expected to be liquid crystalline, an additional analysis of higher concentration solutions is warranted, especially with the use of IDIOM protocols, and will be pursued in the future.

Figure 4a shows the step-size Δh as a function of NaN or SDS concentration, scaled with the corresponding value of CMC. Figure 4a shows that a larger step size is displayed for SDS than NaN at matched scaled concentrations. The values of NaN step size agree reasonably well (to within 1 nm) to that reported by Taylor *et al.*[16] for c_{NaN} = 10 wt.%. Here, the value and the error bar indicate the average and the standard deviation, respectively, that were computed as follows. An average step size was first determined from the values measured at each of the transitions in the thickness evolution plot of a single run. Then, the final value was obtained by averaging such values obtained for at least three (and up to seven) separate single foam film drainage experiments,

and for multiple concentrations, the step size values were verified using independent measurements by coauthors. Thus, the plotted error bars are based on the standard deviation obtained from at least a dozen or more step size values if more than three transitions occur.

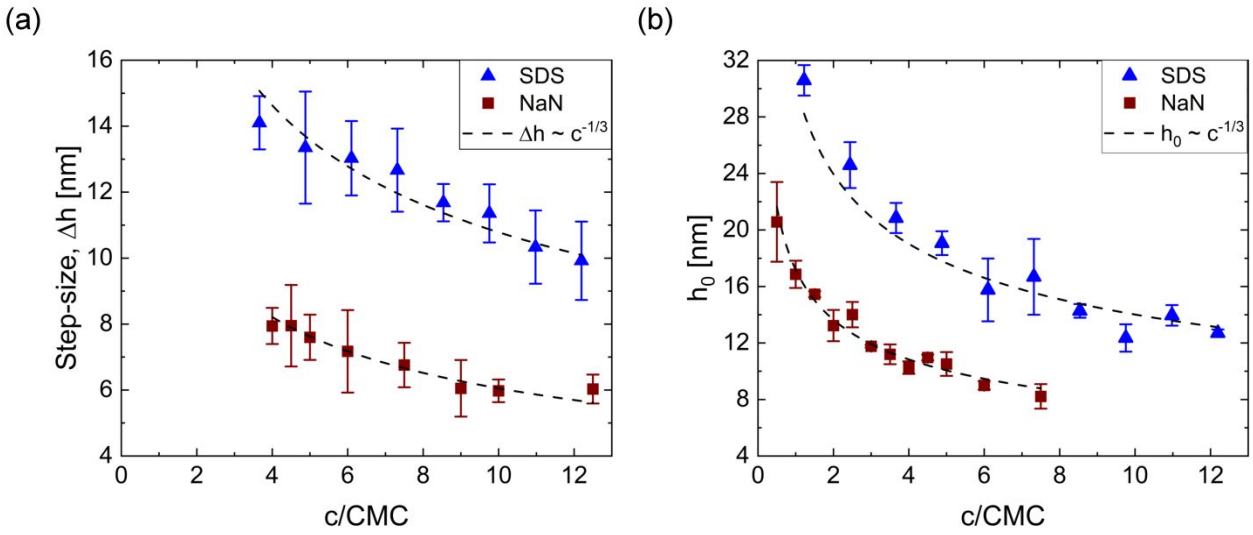

Figure 4. Variation of step-size Δ*h* and layer h_0 thickness as a function of the dimensionless surfactant concentration *c*/CMC. (a) Step-size Δ*h* plotted as a function of dimensionless NaN or SDS concentration, *c*/CMC. **(b)** Terminal thickness, h_0 as a function of scaled concentration *c*/CMC. The dashed lines show the inverse cube root scaling.

The step size decreases with NaN concentration and displays an inverse cubic root law, $\Delta h \sim c^{-1/3}$ reported before for anionic (SDS), cationic (CTAB, CPC), and nonionic surfactants.[20, 22, 26, 38-42, 47, 52, 53, 90] Interparticle distance as a function of volume fraction of packed hard spheres or particles that equals periodicity in the direct measurement of surface forces and simulations, also displays the inverse cubic root scaling.[38, 47, 91-96] We recently compared step size measured in foam film studies to intermicellar distance measured using small-angle X-ray scattering (SAXS) for aqueous SDS solutions, and we showed that intermicellar distance and interactions present in foam films correlate with those in bulk solutions governed by screened Coloumb interactions.[20] This comparison, as well as the agreement between the experimentally-observed domain expansion dynamics and IDIOM-enabled characterization of nanoscopic topography (ridges, mesas, hills,

and gullies) and the theoretical results that consider micellar solutions to be liquid-like and incorporate confinement-induced layering via $\Pi_{OS}(h)$ term, support the hydrodynamic mechanism for stratification.[27, 28, 34, 35, 43, 97, 98]

Figure 4b displays the variation of terminal thickness, h_0 as a function of scaled concentration micellar foam films formulated with aqueous solutions of NaN and SDS, respectively. Like step size, the terminal thickness exhibits the inverse cubic root dependence with $h_0 \sim c^{-1/3}$ and the values are larger for SDS at matched scaled concentrations. Further, the values of h_0 are larger than the values of step-size Δh for both NaN and SDS and can be measured at lower c/CMC values even if only one flat region with constant thickness is manifested. The measured values of terminal thickness, h_0 display good agreement with the values reported by Anachkov et al.[42] but similar comparisons are not possible for NaN. The significant differences in concentration-dependent values of surface tension, step-size Δh, and terminal film thickness h_0 between NaN and SDS arise due to the corresponding differences in the magnitude and range of their intermolecular as well as intermicellar interactions. The presence of a cycloalkane (cyclopentane in our case) group in the hydrophobic tail of NaN in contrast with the linear alkyl chain of 12 carbons in SDS influences tail-tail interactions and packing behavior. The headgroups of SDS and NaN interact via a screened Coulomb potential due to their anionic surface charge, and the electrostatic double layer is populated by positively charged sodium (Na) counterions.[71, 72] A smaller tail size is expected to give a smaller micelle size for NaN and a lower aggregation number N_{agg} at matched c/CMC, and correspondingly, this leads to lower intermicellar distances and lower step size.

CONCLUSIONS

We experimentally found answers to the three primary quests underlying our studies of aqueous NaN foam films. We find foam films formed with aqueous NaN solutions with c/CMC $\leq$ 12.5 stratify, the concentration-dependent variation in step size compares with the scaling obtained for spherical micelle formers like SDS (or $\Delta h \sim c^{-1/3}$) and lastly, the features of nanoscopic topography and underlying surface forces, manifested for NaN films are quite similar to observations previously reported for the micellar foam films formed with salt-added aqueous SDS solutions. The micellar foam films formed by aqueous NaN solutions with concentrations $c_{NaN} \leq$ 12.5 wt.% (c_{NaN}/CMC $\leq$ 12.5) exhibit the characteristic step-wise thinning in the measurement of time-dependent variation in the average local foam film thickness. The ultrathin NaN foam films (h < 100 nm) display coexisting thick-thin flat regions that appear as distinct shades of gray in reflected light microscopy. The thickness maps created using IDIOM (interferometry digital imaging optical microscopy) protocols reveal rich nanoscopic topography, including the formation of nanoridges and mesas. Both step-size, Δh and terminal film thickness h_0 at matched relative concentration are larger in magnitude for SDS solutions. The topographical maps for NaN foam films exhibit the formation of isolated mesas, observed previously for stratified films formed with bile salts and SDS in the presence of salt, indicating that the possibility of higher polydispersity in shape and size of micelles than observed for salt-free SDS.

Significant differences in concentration-dependent values of surface tension, step-size Δh, and terminal film thickness h_0 between NaN and SDS arise due to the corresponding differences in the magnitude and range of their intermolecular as well as intermicellar interactions. The critical micelle concentration (CMC) in aqueous NaN solutions was measured to be c_{NaN} = 1 wt.% using maximum bubble pressure tensiometry and pendant drop tensiometry. The measured value is

relatively close to the values reported in the literature for NaN solutions procured from a commercial source. Though the chemical structure and composition of NaNs obtained from oil sands processed water (OSPW) are likely to be distinct from the commercial NaN used in this study, we envision that the use of similar methods (tensiometry and IDIOM protocols) would prove useful at least as diagnostic tools to determine the variations in concentration and interactions of the NaN micelles, and inspire the exploration of mixed micellar systems, left mostly unexplored in the published stratification studies. We anticipate that our investigations of stratification in the NaN foam films will provide a crucial step forward in characterization and understanding of the influence of interfacially-adsorbed and micellar NaN in stabilizing foams and emulsions and the potential remediation strategies for oil sands processed water (OSPW).

ACKNOWLEDGEMENTS

We acknowledge the funding support by NSF-CBET 1806011 and the UIC College of Engineering. Additionally, the TA support offered to student coauthors by Chemical Engineering and by the School of Chemistry at UIC. We acknowledge discussions with UIC ODES-lab members and comments on the manuscript by Dr. Naveen Reddy, University of Hasselt, Belgium and comments and discussions with our collaborators Dr. Shang Gao and Dr. Samanvaya Srivastava, UCLA. WY works at Fresenius Kabi, Chicago, IL and Dr. YZ works at 10X Genomics, San Francisco Bay Area, CA.

REFERENCES

1. I. Cantat, S. Cohen-Addad, F. Elias, F. Graner, R. Höhler and O. Pitois, *Foams: Structure and Dynamics*, Oxford University Press, 2013.
2. D. L. Weaire and S. Hutzler, *The Physics of Foams*, Oxford University Press, 1999.

3. K. J. Mysels, S. Frankel and K. Shinoda, *Soap films: Studies of their Thinning and a Bibliography*, Pergamon Press, 1959.
4. E. Chatzigiannakis, N. Jaensson and J. Vermant, *Curr. Opin. Colloid Interface Sci.*, 2021, 101441.
5. J. A. Brient, P. J. Wessner and M. N. Doyle, *Kirk-Othmer Encyclopedia of Chemical Technology*, 2000.
6. J. Czarnecki, B. Radoev, L. L. Schramm and R. Slavchev, *Adv. Colloid Interface Sci.*, 2005, **114**, 53-60.
7. G. Horvath-Szabo, J. Czarnecki and J. Masliyah, *J. Colloid Interface Sci.*, 2001, **236**, 233-241.
8. M. H. Mohamed, L. D. Wilson, K. M. Peru and J. V. Headley, *J. Colloid Interface Sci.*, 2013, **395**, 104-110.
9. L. L. Schramm, E. N. Stasiuk and M. MacKinnon, *Surfactants in Athabasca Oil Sands Slurry Conditioning, Flotation Recovery, and Tailings Processes*, Cambridge University Press: Cambridge, 2000.
10. P. Juyal, M. M. Mapolelo, A. Yen, R. P. Rodgers and S. J. Allenson, *Energy Fuels*, 2015, **29**, 2342-2350.
11. G. J. Hirasaki, C. A. Miller and M. Puerto, *SPE Journal*, 2011, **16**, 889-907.
12. S. Gao, K. Moran, Z. Xu and J. Masliyah, *J. Phys. Chem. B*, 2010, **114**, 7710-7718.
13. I. K. Shaik, J. Song, S. L. Biswal, G. J. Hirasaki, P. K. Bikkina and C. P. Aichele, *Journal of Petroleum Science and Engineering*, 2020, **185**, 106567.
14. C. Li, L. Fu, J. Stafford, M. Belosevic and M. G. El-Din, *Sci. Total Environ.*, 2017, **601**, 1785-1802.
15. S. D. Taylor, J. Czarnecki and J. Masliyah, *J. Colloid Interface Sci.*, 2005, **282**, 499-502.
16. S. D. Taylor, J. Czarnecki and J. Masliyah, *J. Colloid Interface Sci.*, 2006, **299**, 283-290.
17. K. Moran and J. Czarnecki, *Colloids Surf. A Physicochem. Eng. Asp.*, 2007, **292**, 87-98.
18. D. Ćirin, M. Poša, L. Grbović, K. Pavlović and B. Vasiljević, *J. Surfactants Deterg.*, 2015, **18**, 83-89.
19. W. Mingqing, Ph. D. , Research Institute of Petroleum Processing, Beijing., 1997.
20. C. Ochoa, S. Gao, S. Srivastava and V. Sharma, *Proc. Natl. Acad. Sci. U.S.A.*, 2021, **118**, e2024805118.
21. Y. Zhang and V. Sharma, *Soft Matter*, 2015, **11**, 4408-4417.
22. Y. Zhang, S. Yilixiati, C. Pearsall and V. Sharma, *ACS Nano*, 2016, **10**, 4678-4683.
23. E. S. Johonnott, *Philosophical Magazine Series 6*, 1906, **11**, 746-753.
24. J. Perrin, *Ann. Phys. (Paris)*, 1918, **10**, 160-184.
25. J. Perrin, in *Nobel Lectures, Physics 1922-1941*, Elsevier Publishing Company, Amsterdam, 1965.
26. H. G. Bruil and J. Lyklema, *Nature Physical Science*, 1971, **233**, 19.
27. Y. Zhang and V. Sharma, *Langmuir*, 2018, **34**, 1208-1217.
28. Y. Zhang and V. Sharma, *Langmuir*, 2018, **34**, 7922–7931.
29. S. Yilixiati, R. Rafiq, Y. Zhang and V. Sharma, *ACS Nano*, 2018, **12**, 1050-1061.
30. S. Yilixiati, E. Wojcik, Y. Zhang and V. Sharma, *Mol. Sys. Des. Eng.*, 2019, **4**, 626-638.
31. J. Lee, A. Nikolov and D. Wasan, *J. Colloid Interface Sci.*, 2017, **496**, 60-65.
32. J. Lee, A. D. Nikolov and D. T. Wasan, *J. Colloid Interface Sci.*, 2017, **487**, 217-222.
33. V. Bergeron, *J. Phys.: Condens. Matter*, 1999, **11**, R215-R238.
34. V. Bergeron, A. I. Jimenez-Laguna and C. J. Radke, *Langmuir*, 1992, **8**, 3027-3032.
35. V. Bergeron and C. J. Radke, *Langmuir*, 1992, **8**, 3020-3026.

36. A. A. Sonin and D. Langevin, *Europhys. Lett.*, 1993, **22**, 271.
37. D. Langevin and A. A. Sonin, *Adv. Colloid Interface Sci.*, 1994, **51**, 1-27.
38. D. T. Wasan and A. D. Nikolov, *Curr. Opin. Colloid Interface Sci.*, 2008, **13**, 128-133.
39. D. T. Wasan, A. D. Nikolov, P. A. Kralchevsky and I. B. Ivanov, *Colloids Surf.*, 1992, **67**, 139-145.
40. A. D. Nikolov, D. T. Wasan, P. A. Kralchevsky and I. B. Ivanov, Kyoto, Japan, 1988.
41. A. D. Nikolov and D. T. Wasan, *J. Colloid Interface Sci.*, 1989, **133**, 1-12.
42. S. E. Anachkov, K. D. Danov, E. S. Basheva, P. A. Kralchevsky and K. P. Ananthapadmanabhan, *Adv. Colloid Interface Sci.*, 2012, **183**, 55-67.
43. P. Heinig, C. M. Beltrán and D. Langevin, *Phys. Rev. E.*, 2006, **73**, 051607.
44. Z. Lalchev, R. Todorov and D. Exerowa, *Curr. Opin. Colloid Interface Sci.*, 2008, **13**, 183-193.
45. P. J. Beltramo and J. Vermant, *ACS Omega*, 2016, **1**, 363-370.
46. C. M. Beltrán and D. Langevin, *Phys. Rev. Lett.*, 2005, **94**, 217803.
47. R. von Klitzing, E. Thormann, T. Nylander, D. Langevin and C. Stubenrauch, *Adv. Colloid Interface Sci.*, 2010, **155**, 19-31.
48. S. I. Kemal, C. A. U. Ortiz and V. Sharma, *Mol. Sys. Des. Eng.*, 2021, **6**, 520-533.
49. C. V. Boys, *Soap Bubbles: Their Colours and the Forces Which Mold Them*, Society for Promoting Christian Knowledge, London, 1912.
50. G. Gochev, D. Platikanov and R. Miller, *Adv. Colloid Interface Sci.*, 2016, **233**, 115-125.
51. A. Sheludko, *Adv. Colloid Interface Sci.*, 1967, **1**, 391-464.
52. O. Krichevsky and J. Stavans, *Phys. Rev. Lett.*, 1995, **74**, 2752.
53. O. Krichevsky and J. Stavans, *Phys. Rev. E.*, 1997, **55**, 7260.
54. E. D. Manev, S. V. Sazdanova and D. T. Wasan, *J. Colloid Interface Sci.*, 1984, **97**, 591-594.
55. R. Höhler, J. Seknagi and A. Kraynik, *Soft Matter*, 2021.
56. N. Yanagisawa, M. Tani and R. Kurita, *Soft Matter*, 2021, **17**, 1738-1745.
57. S. Cohen-Addad, R. Hohler and O. Pitois, *Ann. Rev. Fluid. Mech.*, 2013, **45**, 241-267.
58. P. M. Kruglyakov, S. I. Karakashev, A. V. Nguyen and N. G. Vilkova, *Curr. Opin. Colloid Interface Sci.*, 2008, **13**, 163-170.
59. S. I. Karakashev, *Exp. Fluids*, 2017, **58**, 1-40.
60. V. C. Suja, M. Rodríguez-Hakim, J. Tajuelo and G. G. Fuller, *Adv. Colloid Interface Sci.*, 2020, 102295.
61. H. A. Stone, S. A. Koehler, S. Hilgenfeldt and M. Durand, *J. Phys. Conden. Mat.*, 2003, **15**, S283-S290.
62. L. Keal, V. Lapeyre, V. Ravaine, V. Schmitt and C. Monteux, *Soft Matter*, 2017, **13**, 170-180.
63. E. Chatzigiannakis and J. Vermant, *Soft Matter*, 2021, **17**, 4790-4803.
64. E. Hermans, M. S. Bhamla, P. Kao, G. G. Fuller and J. Vermant, *Soft Matter*, 2015, **11**, 8048-8057.
65. L. Saulnier, L. Champougny, G. Bastien, F. Restagno, D. Langevin and E. Rio, *Soft Matter*, 2014, **10**, 2899-2906.
66. D. Langevin, *Adv. Colloid Interface Sci.*, 2020, **275**, 102075.
67. N. Denkov, S. Tcholakova and N. Politova-Brinkova, *Curr. Opin. Colloid Interface Sci.*, 2020.
68. J. Ferreira, A. Mikhailovskaya, A. Chenneviere, F. Restagno, F. Cousin, F. Muller, J. Degrouard, A. Salonen and E. F. Marques, *Soft Matter*, 2017, **13**, 7197-7206.
69. B. V. Derjaguin, N. V. Churaev and V. M. Muller, *Surface Forces*, Springer, New York, 1987.

70. D. Fennell Evans and H. Wennerström, *The Colloidal Domain: Where Physics, Chemistry, Biology, and Technology Meet*, Wiley-VCH: New York, 2nd edn., 1999.
71. J. N. Israelachvili, *Intermolecular and Surface Forces*, Academic Press, 3rd edn., 2011.
72. J. Israelachvili and M. Ruths, *Langmuir*, 2013, **29**, 9605-9619.
73. P. A. Kralchevsky and N. D. Denkov, *Chem. Phys. Lett.*, 1995, **240**, 385-392.
74. P. A. Kralchevsky, A. D. Nikolov, D. T. Wasan and I. B. Ivanov, *Langmuir*, 1990, **6**, 1180-1189.
75. A. Patist, J. R. Kanicky, P. K. Shukla and D. O. Shah, *J. Colloid Interface Sci.*, 2002, **245**, 1-15.
76. R. Itri and L. Q. Amaral, *J. Phys. Chem.*, 1991, **95**, 423-427.
77. R. Itri, L. Q. Amaral and P. Mariani, *Phys. Rev. E.*, 1996, **54**, 5211.
78. J. Chen, L. He, X. Luo and C. Zhang, *Colloids Surf. A Physicochem. Eng. Asp.*, 2018, **553**, 432-438.
79. C. A. U. Ortiz, University of Illinois at Chicago, 2017.
80. N. C. Christov, K. D. Danov, P. A. Kralchevsky, K. P. Ananthapadmanabhan and A. Lips, *Langmuir*, 2006, **22**, 7528-7542.
81. V. Bergeron and C. J. Radke, *Colloid. Polym. Sci.*, 1995, **273**, 165-174.
82. D. Exerowa, T. Kolarov and K. Khristov, *Colloids Surf.*, 1987, **22**, 161-169.
83. E. A. Adelizzi and S. M. Troian, *Langmuir*, 2004, **20**, 7482-7492.
84. S. Berg, E. A. Adelizzi and S. M. Troian, *Langmuir*, 2005, **21**, 3867-3876.
85. J. M. Frostad, D. Tammaro, L. Santollani, S. B. de Araujo and G. G. Fuller, *Soft Matter*, 2016, **12**, 9266-9279.
86. V. C. Suja, J. Sentmanat, G. Hofmann, C. Scales and G. G. Fuller, *Scientific Reports*, 2020, **10**, 1-8.
87. K. J. Mysels, *Langmuir*, 1986, **2**, 423-428.
88. E. S. Basheva, K. D. Danov and P. A. Kralchevsky, *Langmuir*, 1997, **13**, 4342-4348.
89. P. Oswald and P. Pieranski, *Smectic and Columnar Liquid Crystals: Concepts and Physical Properties Illustrated by Experiments*, CRC Press, 2005.
90. K. D. Danov, E. S. Basheva, P. A. Kralchevsky, K. P. Ananthapadmanabhan and A. Lips, *Adv. Colloid Interface Sci.*, 2011, **168**, 50-70.
91. S. H. L. Klapp, S. Grandner, Y. Zeng and R. von Klitzing, *J. Phys.: Condens. Matter*, 2008, **20**.
92. S. H. L. Klapp, S. Grandner, Y. Zeng and R. von Klitzing, *Soft Matter*, 2010, **6**, 2330-2336.
93. M. Ludwig and R. von Klitzing, *Curr. Opin. Colloid Interface Sci.*, 2020.
94. M. Ludwig, M. U. Witt and R. von Klitzing, *Adv. Colloid Interface Sci.*, 2019, **269**, 270-276.
95. Y. Zeng, S. Grandner, C. L. P. Oliveira, A. F. Thunemann, O. Paris, J. S. Pedersen, S. H. L. Klapp and R. von Klitzing, *Soft Matter*, 2011, **7**, 10899-10909.
96. Y. Zeng, S. Schön and R. von Klitzing, *J. Colloid Interface Sci.*, 2015, **449**, 522-529.
97. M. L. Pollard and C. J. Radke, *J. Chemical Physics*, 1994, **101**, 6979-6991.
98. M. L. Pollard and C. J. Radke, *AlChE J.*, 1996, **42**, 2005-2013.